Electronic Supplementary Material (ESI) for Energy & Environmental Science.
This journal is © The Royal Society of Chemistry 2022

Electronic Supplementary Information (ESI)

A Structurally Simple Linear Conjugated Polymer toward Practical Application of Organic Solar Cells

Bingyan Yin, Shuting Pang, Zhili Chen, Wanyuan Deng, Zhitian Liu, Chunhui Duan, Fei Huang, and Yong Cao*

1. Experimental details

General information: The synthesis route of PTTzF is shown in Figure S1. The compounds 3-(2-hexyldecyl)-thiophene (2), 2-bromo-3-(2-hexyldecyl)-thiophene (3), 3-(2-hexyldecyl)-thiophene-2-carbaldehyde (4), 2,5-bis-[3-(2-hexyldecyl)-thiophen-2-yl]-thiazolo[5,4-d]thiazole (5), 2,5-bis-[5-bromo-3-(2-hexyldecyl)-thiophen-2-yl]-thiazolo[5,4-d]thiazole (M1) were synthesized according to the procedures reported in literatures.[1, 2] 3,4-Difluoro-2,5-bis(trimethylstannyl)thiophene (M2) and $Pd_2(dba)_3$ was purchased from Derthon and Strem, respectively. The other chemicals and solvents were purchased from commercial sources (Innochem, Energy Chemical or Acros) and used as received unless otherwise indicated.

Polymerization of PTTzF (M_n = 27 kDa): In the degassed solution of M1 (136.9 mg, 0.15 mmol) and M2 (66.8 mg, 0.15 mmol) in anhydrous chlorobenzene (1.8 mL) and *N,N*-dimethylformamide (0.2 mL), $Pd_2(dba)_3$ (2.7 mg, 0.003 mmol) and P(*o*-tol)$_3$ (7.3 mg, 0.024 mmol) were added under nitrogen protection. The mixture was stirred at 120 ℃ for 2 hours at the initial stage. Next, the reaction temperature was decreased and kept at 80 ℃ for 12 hours. Then, the reaction temperature was increased to 120 ℃ again and maintained for 24 hours. After that, 2-(tributylstannyl)thiophene and 2-bromothiophene were sequentially added to the reaction with 2 hours interval. After cooling to room temperature, the reaction mixture was precipitated in methanol and filtered through a Soxhlet thimble. The precipitation was subjected to Soxhlet extraction with methanol, acetone, hexane, dichloromethane, chloroform sequentially under nitrogen protection. The chloroform fraction was concentrated under

reduced pressure and precipitated in methanol to obtain the polymer PTTzF (120 mg, yield = 88%). M_n = 27 kDa, $Đ_M$ = 2.26.

Polymerization of PTTzF (M_n = 30 kDa): In the degassed solution of M1 (182.6 mg, 0.2 mmol) and M2 (89.1 mg, 0.2 mmol) in anhydrous chlorobenzene (2.7 mL), $Pd_2(dba)_3$ (3.6 mg, 0.004 mmol) and P(*o*-tol)$_3$ (9.7 mg, 0.032 mmol) were added under nitrogen protection. Then the mixture was stirred at 120 ℃ for 72 hours. After that, 2-(tributylstannyl)thiophene and 2-bromothiophene were sequentially added to the reaction with 2 hours interval. The post-treatment procedure is the same as described above. Ultimately the chloroform fraction was concentrated under reduced pressure and precipitated in methanol to obtain the polymer PTTzF (178 mg, yield = 98%). M_n = 30 kDa, $Đ_M$ = 2.20.

Polymerization of PTTzF (M_n = 32 kDa): In the degassed solution of M1 (182.6 mg, 0.2 mmol) and M2 (89.1 mg, 0.2 mmol) in anhydrous chlorobenzene (4 mL), $Pd_2(dba)_3$ (3.6 mg, 0.004 mmol) and P(*o*-tol)$_3$ (9.7 mg, 0.032 mmol) were added under nitrogen protection. The mixture was stirred at 120 ℃ for 2 hours at the initial stage. Next, the reaction temperature was decreased and kept at 80 ℃ for 12 hours. Then, the reaction temperature was increased to 120 ℃ again and maintained for 24 hours. After that, 2-(tributylstannyl)thiophene and 2-bromothiophene were sequentially added to the reaction with 2 hours interval. The post-treatment procedure is the same as described above. Ultimately the chloroform fraction was concentrated under reduced pressure and precipitated in methanol to obtain the polymer PTTzF (169 mg, yield = 93%). M_n = 32 kDa, $Đ_M$ = 1.89.

Polymerization of PTTzF (M_n = 38 kDa): In the degassed solution of M1 (91.3 mg, 0.1 mmol) and M2 (44.5 mg, 0.1 mmol) in anhydrous chlorobenzene (1.3 mL), $Pd_2(dba)_3$ (1.83 mg, 0.002 mmol) and P(*o*-tol)$_3$ (4.8 mg, 0.016 mmol) were added under nitrogen protection. The mixture was stirred at 120 ℃ for 2 hours at the initial stage. Next, the reaction temperature was decreased and kept at 80 ℃ for 12 hours. Then, the reaction temperature was increased to 120 ℃ again and maintained for 24 hours. After that, 2-(tributylstannyl)thiophene and 2-

bromothiophene were sequentially added to the reaction with 2 hours interval. The polymer post-processing procedure is the same as described above. Ultimately the chloroform fraction was concentrated under reduced pressure and precipitated in methanol to obtain the polymer PTTzF (83 mg, yield = 92%). M_n = 38 kDa, $Đ_M$ = 1.87.

2. Measurements and characterizations

Gel permeation chromatography (GPC): The molecular weights of PTTzF were determined by Agilent Technologies PL-GPC 220 high-temperature chromatography in 1,2,4-trichlorobenzene (TCB) at 140 °C using a calibration curve of polystyrene standards.

Thermogravimetric analysis (TGA): The TGA measurements were carried out with a NETZSCH (TG209F3) apparatus at a heating rate of 20 °C min^{-1} under nitrogen atmosphere.

Differential scanning calorimetry (DSC): The DSC measurements were performed on a NETZSCH (DSC200F3) apparatus under a nitrogen atmosphere with a heating/cooling rate of 10/20 °C min^{-1} for the first cycle and a heating/cooling rate of 10/40 °C min^{-1} for the second cycle, respectively.

UV-vis absorption spectra: UV-vis absorption spectra of the polymers in chlorobenzene solutions and as thin films were recorded on a SHIMADZU UV-3600 spectrophotometer. The solution concentration was 0.02 mg mL^{-1}, and the films were spin-coated on glass substrates.

Cyclic voltammetry (CV): Cyclic voltammetry measurements were conducted on a CHI660A electrochemical workstation in a solution of tetrabutylammonium hexafluorophosphate (Bu_4NPF_6, 0.1 mol L^{-1}) in acetonitrile. A glassy carbon, a platinum wire, and an Ag/AgCl electrode were used as working electrode, counter electrode, and reference electrode, respectively. A ferrocene/ferrocenium (Fc/Fc^+) redox couple was used as internal standard and was assigned an absolute energy of –4.8 eV versus vacuum. The HOMO and LUMO energies of materials were determined according to the equation $E_{HOMO} = -(E_{ox\ onset} + 4.8 - E_{Fc/Fc+})$ and $E_{LUMO} = -(E_{red\ onset} + 4.8 - E_{Fc/Fc+})$, where $E_{ox\ onset}$ and $E_{red\ onset}$ are the onsets of oxidation and

reduction potential relative to the measured Fc/Fc^+ redox couple, respectively. The formal potential of Fc/Fc^+ redox couple was found at 0.42 V relative to the Ag/Ag^+ electrode.

Density functional theory (DFT) calculation: The molecular geometry was calculated with Gaussian at B3LY/6-31G (d,p) level. The alkyl chains were replaced with methy to simplify the calculation.

Steady-state photoluminescence (PL): The PL quenching measurements were conducted at an excitation wavelength of 530 nm on a Shimadzu RF-6000 spectrometer.

Atomic force microscopy (AFM): AFM images were obtained by Bruker Multimode 8 Microscope AFM in tapping mode.

Transmission electron microscopy (TEM): TEM images were collected from JEM-2100F transmission electron microscope operated at 200 kV.

Grazing incidence wide-angle X-ray scattering (GIWAXS): The GIWAXS measurements were performed on a Xenocs Xeuss 2.0 system with an Excillum MetalJet-D2 X-ray source. The X-ray beam was operated at 70.0 kV, 2.8570 mA. The wavelength of the X-ray was 1.341 Å. The grazing-incidence angle was set at 0.20 °. Scattering patterns were collected with a DECTRIS PILATUS3 R 1M area detector. The raw GIWAXS data was analyzed by Igor software with Nika package.

3. Device fabrication and characterization

Fabrication of solar cells: The substrates with indium tin oxide (ITO) were cleaned by detergent, sonicated in deionized water, and isopropanol sequentially. After that, the clean substrates were dried in oven at 70 °C. The ITO substrates were subjected to oxygen plasma for 3 minutes. An aqueous solution of PEDOT:PSS (4083) was spin-casted onto the ITO substrate at 4000 rpm for 30 seconds, followed by drying at 150 °C for 15 minutes in air. The substrates were then transferred into a nitrogen-filled glove box. The active layer was fully optimized in terms of solvent additive, thermal annealing temperature and duration, and

donor:acceptor weight ratios. For the optimal binary OSC devices, the polymers and Y6 were dissolved in a solvent mixture of chloroform (CF) and chloronaphthalene (CN) (volume fraction of 0.5%) at a donor concentration of 7.5 mg mL^{-1} (donor:acceptor weight ratio is 1:1.2). The optimal ternary OSC devices were fabricated by introducing [70]PCBM into the optimal binary system with weight ratio of 1:1.2:0.2. The active layers were spin-coated at 2000 rpm. The films were then annealed at 100 °C for ten minutes. Afterwards, an electron transport layer of PNDIT-F3N was spin-coated from a solution (0.5 mg mL^{-1}) at a speed of 2000 rpm for 30 seconds. Finally, a 100 nm Ag was deposited by thermal evaporation in a vacuum chamber at a pressure of 5×10^{-6} Torr with a shadow mask.

Photovoltaic performance measurements: The photovoltaic performances were measured under AM1.5G irradiation (100 mW cm^{-2}) derived from a class solar simulator (Enlitech, Taiwan), which was calibrated by a China General Certification Center-certified reference single-crystal silicon cell (Enlitech). The current density–voltage (*J–V*) curves were recorded with a Keithley 2400 source meter. The device area is 0.0516 cm^{-2}, and the test was performed with a mask aperture which defined an effective area of 0.04 cm^{-2}.

External quantum efficiencies (EQEs): The EQE spectra were measured by a QE system (QE-R3011, Enlitech, Taiwan) with the light intensity calibrated by a standard single-crystal silicon photovoltaic cell (Enlitech).

Light-intensity dependence measurements: The light-intensity dependence measurements were carried out with illumination between 10–100 mW cm^{-2}, which was calibrated by a standard single-crystal silicon solar cell (Enlitech). The current density and voltage were recorded with a Keithley 2400 source meter.

Fabrication and characterization of single-carrier devices: The charge carrier mobilities were measured in single-carrier devices with a structure of ITO/PEDOT:PSS/active layer/MoO_3/Ag for hole-only devices, and a structure of ITO/ZnO/active layer/PNDIT-F3N/Ag

for electron-only devices. The dark current densities were measured by applying a voltage between 0 and 4 V with a Keithley 2400 source meter.

Charge carrier mobility estimation: The charge carrier mobility was estimated by fitting the data acquired from single-carrier devices to a space-charge-limit-current (SCLC) model. The mobility was determined by fitting the dark current according to the Mott-Gurney law that consider a Poole-Frenkel-type dependence of mobility on the electric field, given by the following equation:

$$J = \frac{9}{8}\varepsilon_0\varepsilon_r\mu_0 exp(0.89\gamma\sqrt{V/d}) \quad \text{(S1)}$$

where J is the dark current density, ε_0 is the permittivity of free space, ε_r is the dielectric constant of the polymer which is assumed to be 3 for organic semiconductors, μ_0 is the zero-filed mobility, γ is a parameter that describes the strength of the field-dependence effect, V is voltage drop across the device, and d is the thickness of the active layer. The hole and electron mobilities are extracted with the fit parameters at an electric field (E) of 1.0×10^5 V cm^{-1} by the Murgatroyd equation:

$$\mu = \mu_0 exp(\gamma\sqrt{E}) \quad \text{(S2)}$$

4. Additional figures and tables

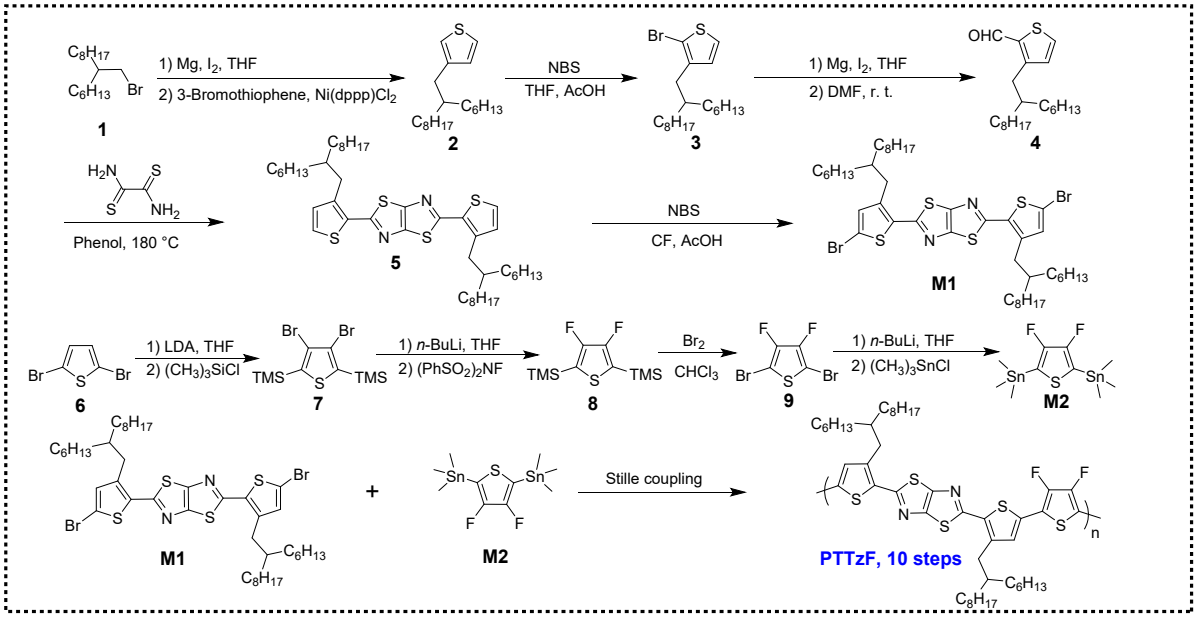

Figure S1. The synthetic route of PTTzF.

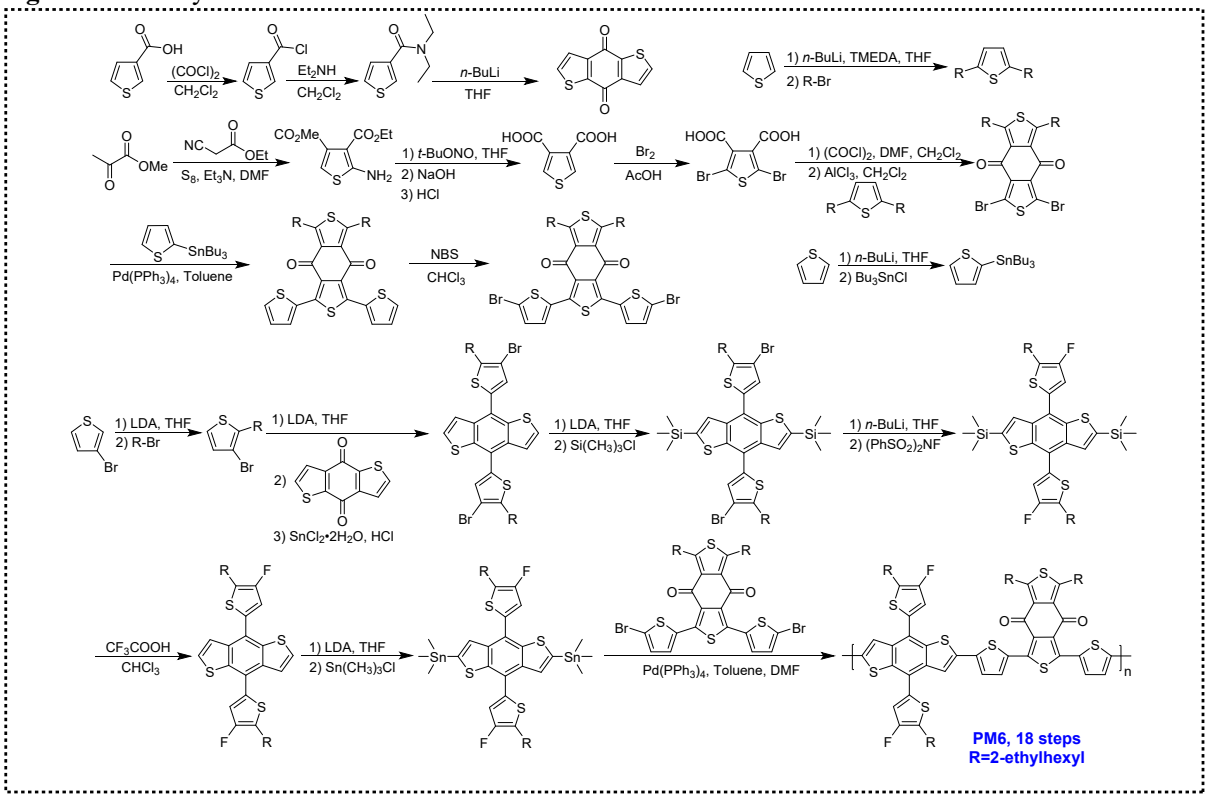

Figure S2. The synthetic route of PM6.[3-6]

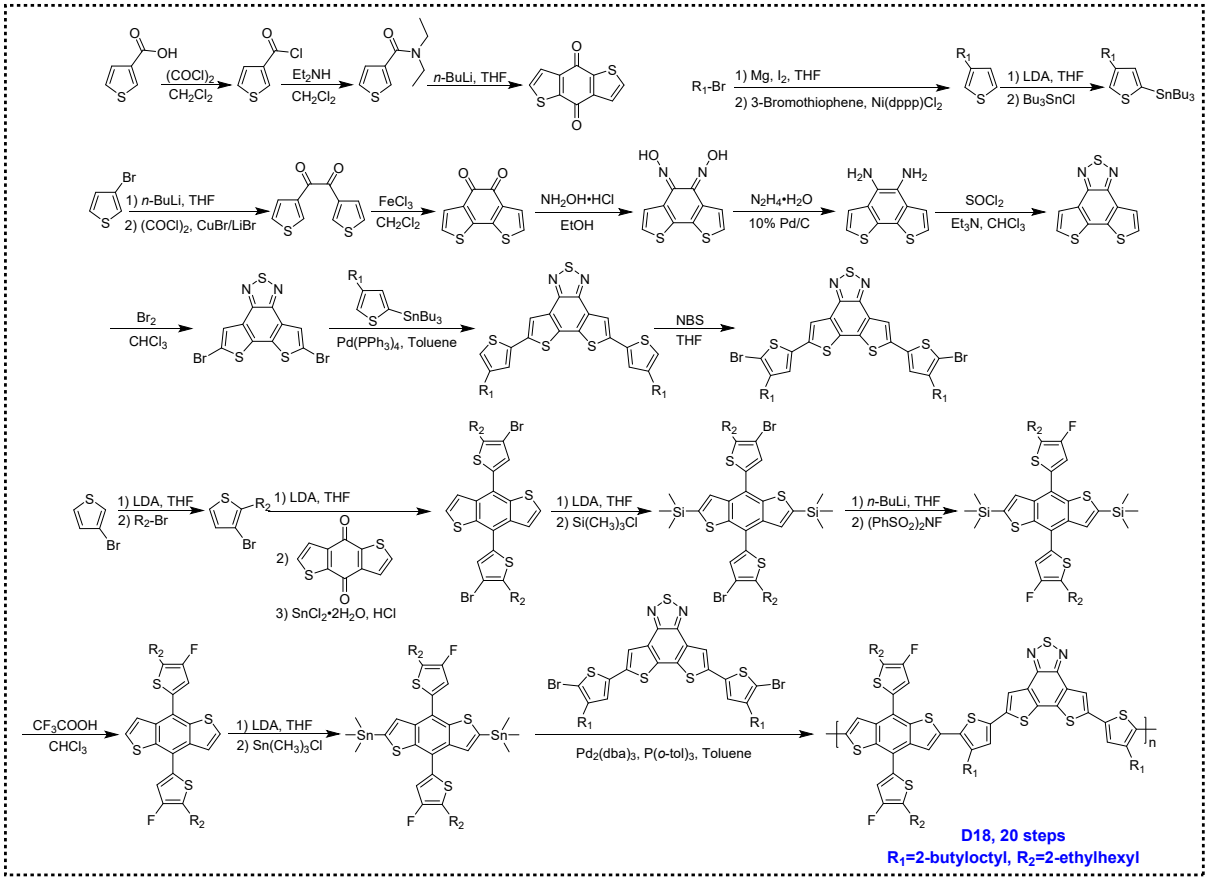

Figure S3. The synthetic route of D18.[4, 7, 8]

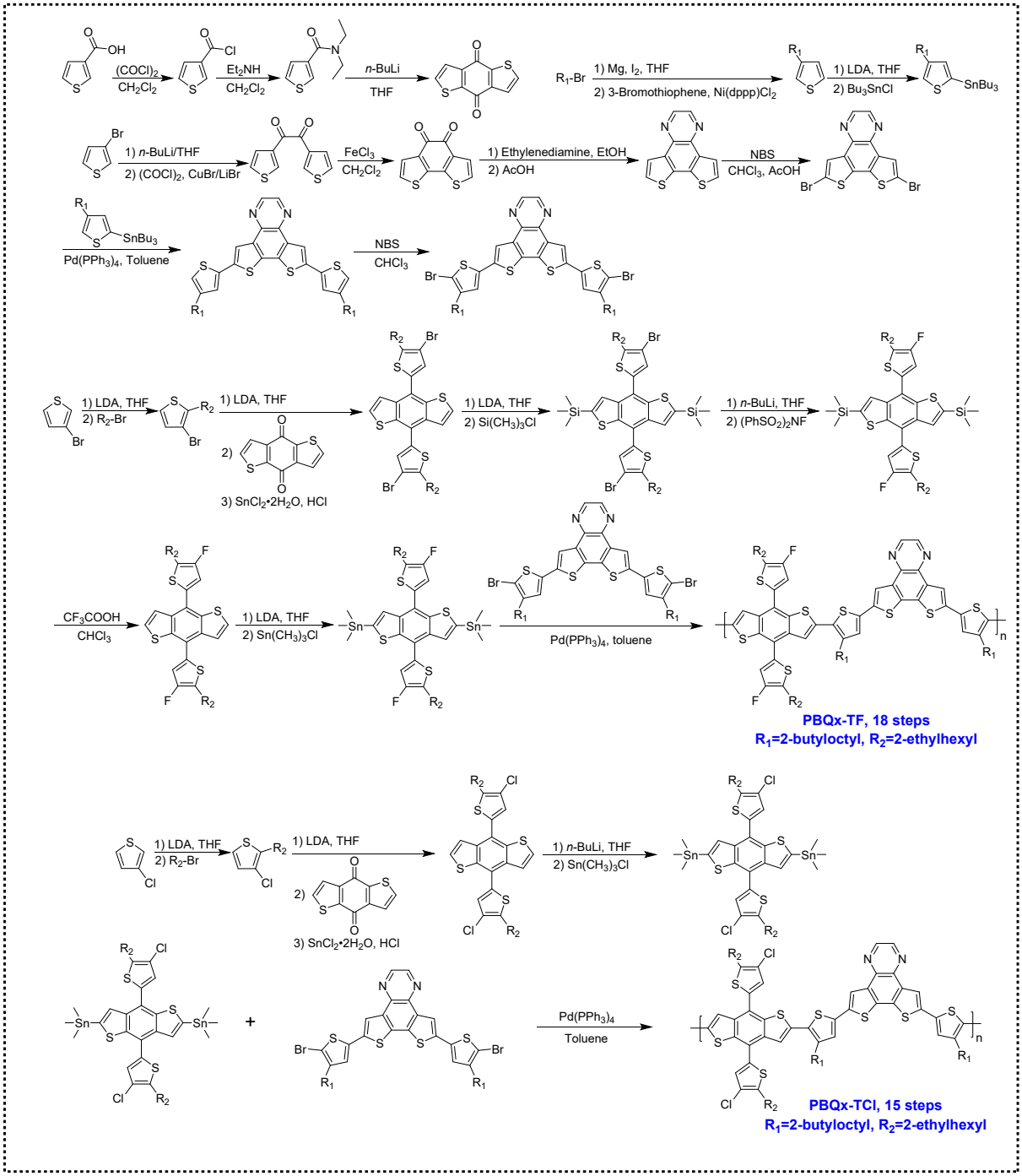

Figure S4. The synthetic route of PBQx-TX, X=F or X=Cl.[4, 9, 10]

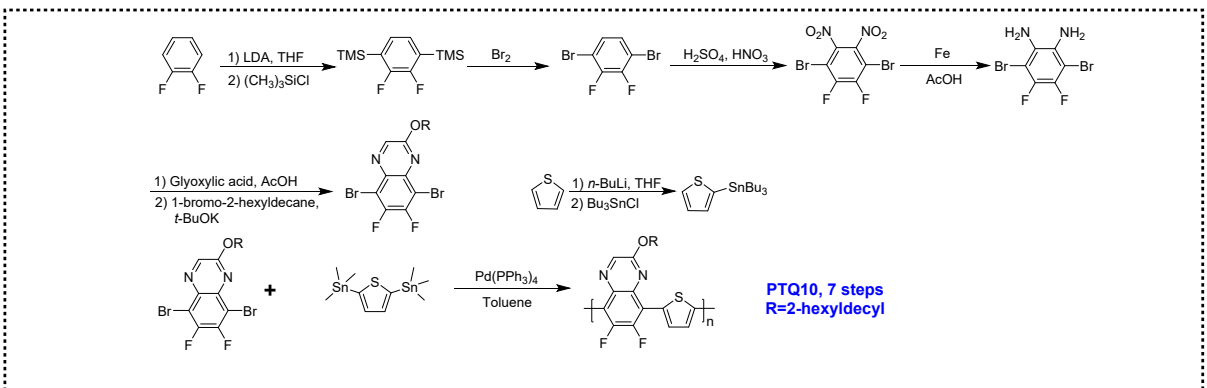

Figure S5. The synthetic route of PTQ10.[11, 12]

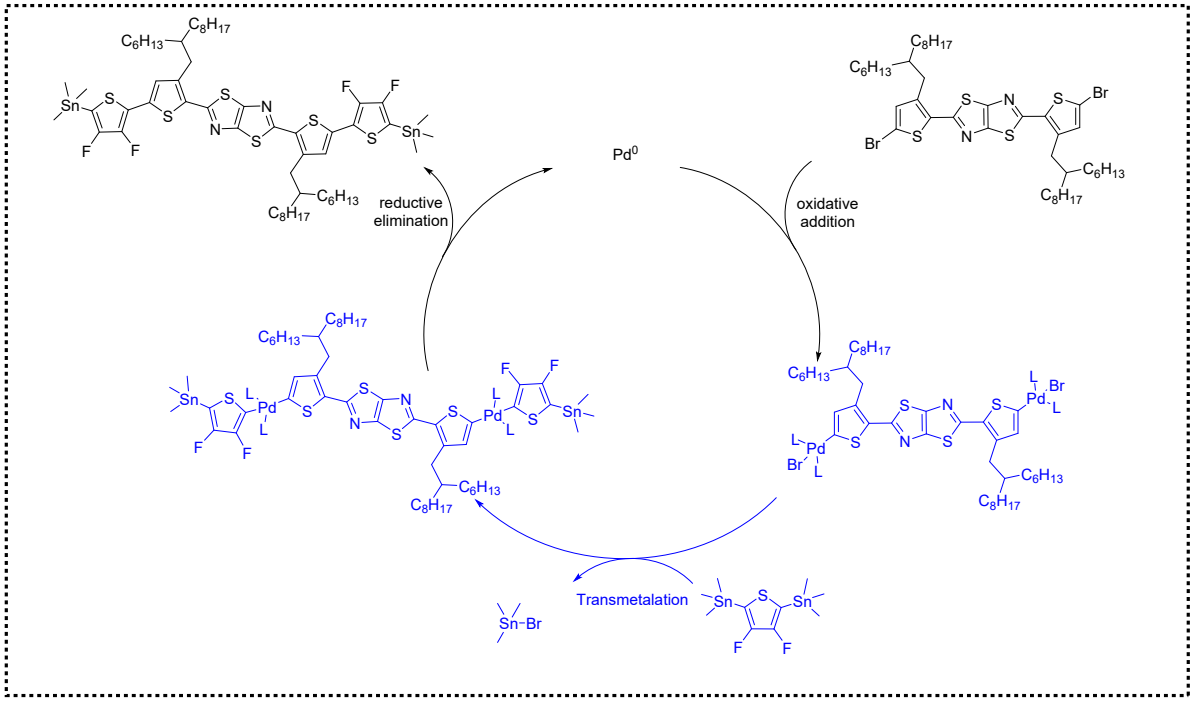

Figure S6. The mechanism of the Stille cross-coupling reaction in the synthesis process of PTTzF.

Table S1. The reaction conditions of the Stille polymerization and number average molecular weights (M_n) of different batches of PTTzF.[a)]

Entry	Catalyst[b)]	Solvent	Monomer concentrationc)	Temperature/time	Yield d) (%)	Mn (kDa)/ĐM
1	$Pd_2(dba)_3$/P(o-tol)$_3$	CB/DMF	0.15 M	120 °C/2 h 80 °C/12 h 120 °C/24 h	88%	27/2.26
2	$Pd_2(dba)_3$/P(o-tol)$_3$	CB	0.15 M	120 °C/72 h	98%	30/2.20
3	$Pd_2(dba)_3$/P(o-tol)$_3$	CB	0.10 M	120 °C/2 h 80 °C/12 h 120 °C/24 h	93%	32/1.89
4	$Pd_2(dba)_3$/P(o-tol)$_3$	CB	0.15 M	120 °C/2 h 80 °C/12 h 120 °C/24 h	92%	38/1.87

[a)] All the crude polymers were extracted successively with methanol, acetone, hexane, dichloromethane, chloroform sequentially under argon protection.
[b)] The catalyst loadings were 2 mol% $Pd_2(dba)_3$ and 16 mol% P(*o*-tol)$_3$ for the entry 1 to 4.
[c)] Monomer concentration was the total concentration of both bis(trimethytin) monomer and dibrominated monomer.
[d)] The yield of polymer fraction extracted by chloroform.

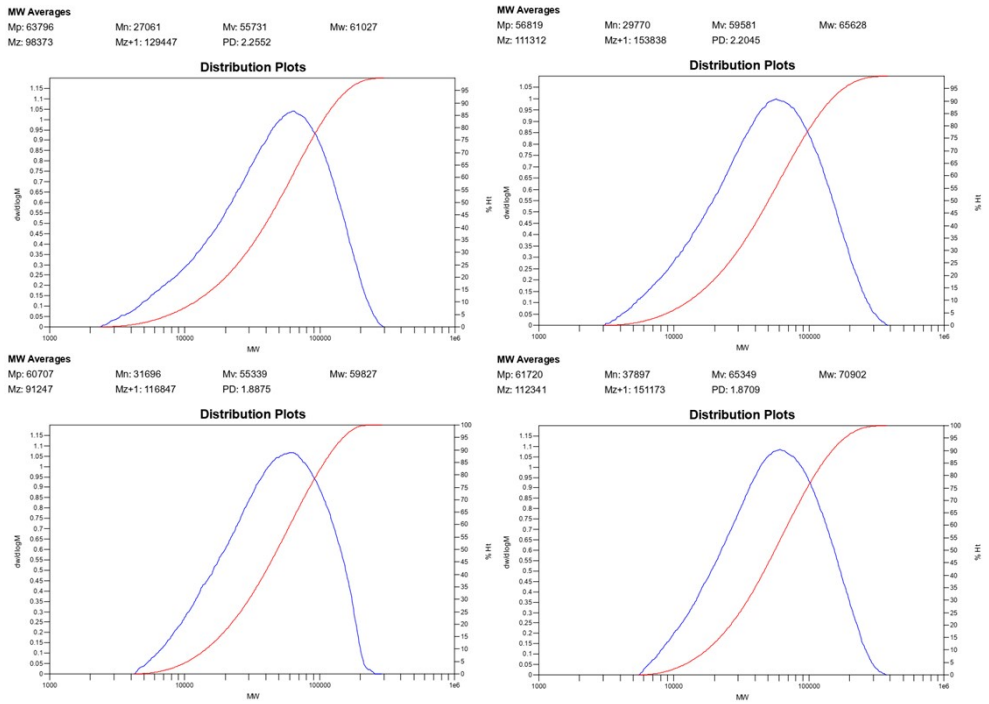

Figure S7. The GPC traces of four different batches of PTTzF under different polymerization conditions.

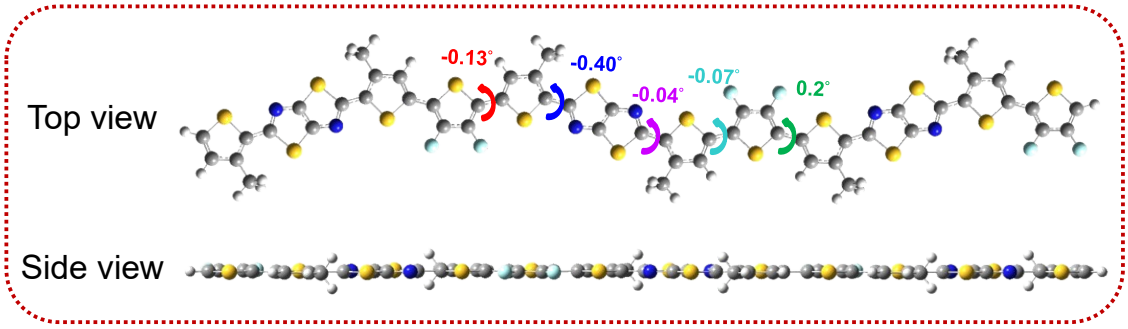

Figure S8. The conformation of PTTzF simulated by DFT calculation based on three repeat units.

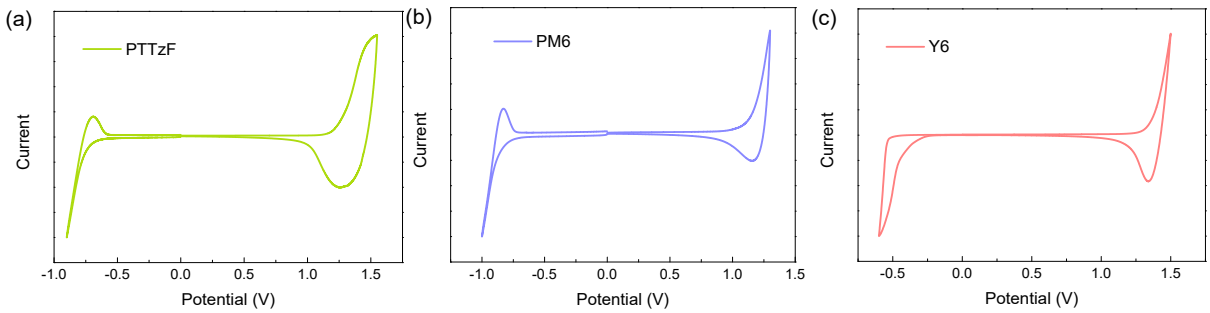

Figure S9. Cyclic voltammetry curves of PTTzF, PM6, and Y6.

Table S2. Photovoltaic parameters of PTTzF:Y6 solar cells under AM1.5G irradiation (100 mW cm^{-2}).

Solvent [v/v]	D:A [w/w]	TA	V_{oc} [V]	J_{sc} [mA cm^{-2}]	FF	PCE [%]
CF	1:1	w/o	0.860	23.73	0.699	14.25
CF (0.5% DIO)			0.838	22.88	0.708	13.57
CF (0.5% DPE)			0.838	23.85	0.689	13.76
CF (0.5% CN)			0.860	23.82	0.737	15.11
CF (0.25% CN)	1:1	w/o	0.865	25.01	0.714	15.44
CF (0.5% CN)			0.866	25.15	0.714	15.55
CF (0.75% CN)			0.861	24.45	0.730	15.38
CF (1% CN)			0.855	20.74	0.609	10.79
CF (0.5% CN)	1:1	w/o	0.869	24.88	0.725	15.68
		80 °C × 5 min	0.855	24.83	0.743	15.86
		100°C × 5 min	0.843	26.15	0.752	16.57
		120°C × 5 min	0.843	25.81	0.751	16.34
CF (0.5% CN)	1:1	100°C × 3 min	0.847	25.31	0.724	15.52
		100°C × 5 min	0.845	26.53	0.737	16.52
		100°C × 10 min	0.844	26.43	0.750	16.73
		100°C × 20 min	0.838	25.53	0.709	15.17
CF (0.5% CN)	1.2:1	100°C × 10 min	0.847	25.31	0.679	14.56
	1:1		0.853	26.30	0.748	16.78
	1:1.2		0.855	26.73	0.757	17.30
	1:1.5		0.854	25.88	0.754	16.67

Table S3. Photovoltaic parameters of PTTzF:Y6:[70]PCBM ternary solar cells under AM1.5G irradiation (100 mW cm^{-2}) with different fraction of [70]PCBM.

PTTzF:Y6:[70]PCBM [w/w]	TA	V_{oc} [V]	J_{sc} [mA cm^{-2}]	FF	PCE [%]
1:1.2:0.15	100 °C × 10 min	0.859	26.55	0.755	17.24
1:1.2:0.2		0.847	27.52	0.773	18.01
1:1.2:0.3		0.858	26.46	0.755	17.25

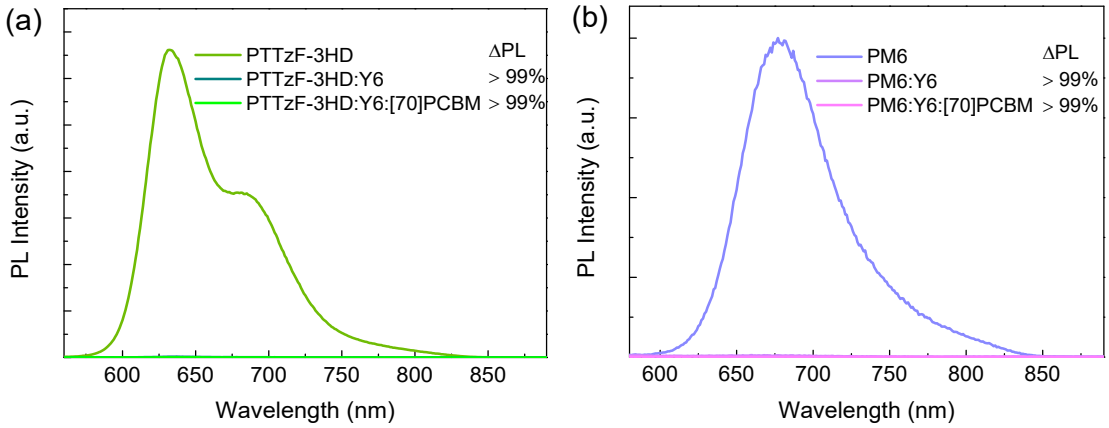

Figure S10. The steady-state photoluminescence spectra of the neat and blend films of PTTzF and PM6 with the excitation wavelength of 530 nm.

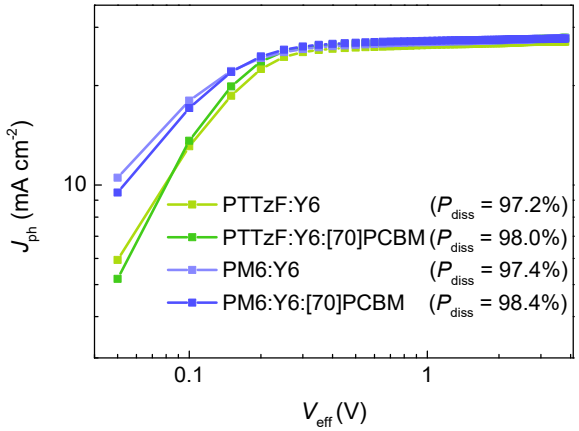

Figure S11. The plots of J_{ph} versus V_{eff} of binary and ternary OSCs based on PTTzF and PM6.

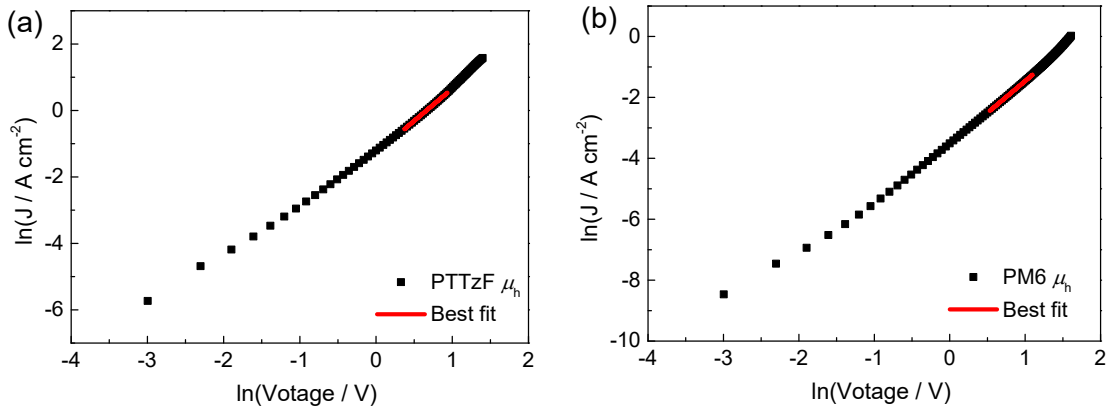

Figure S12. J–V characteristics of the hole-only devices based on the neat films of PTTzF and PM6.

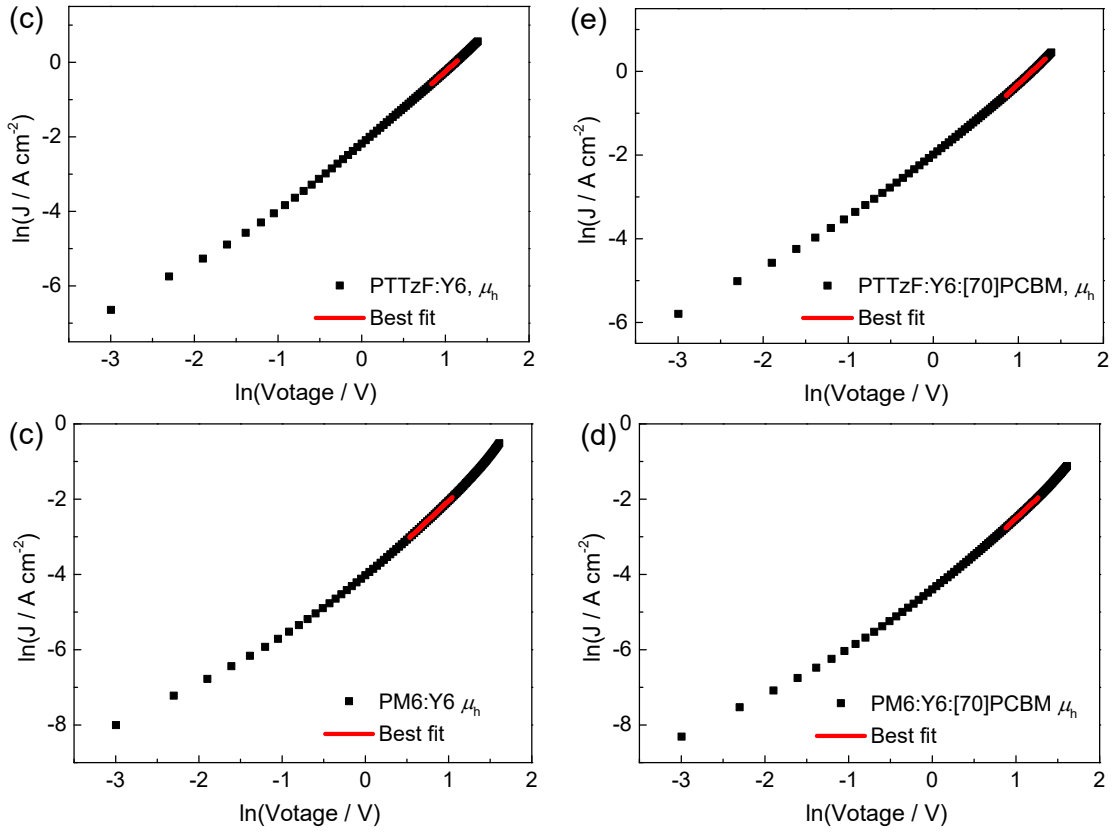

Figure S13. *J–V* characteristics of the hole-only devices based on the blend films of PTTzF and PM6.

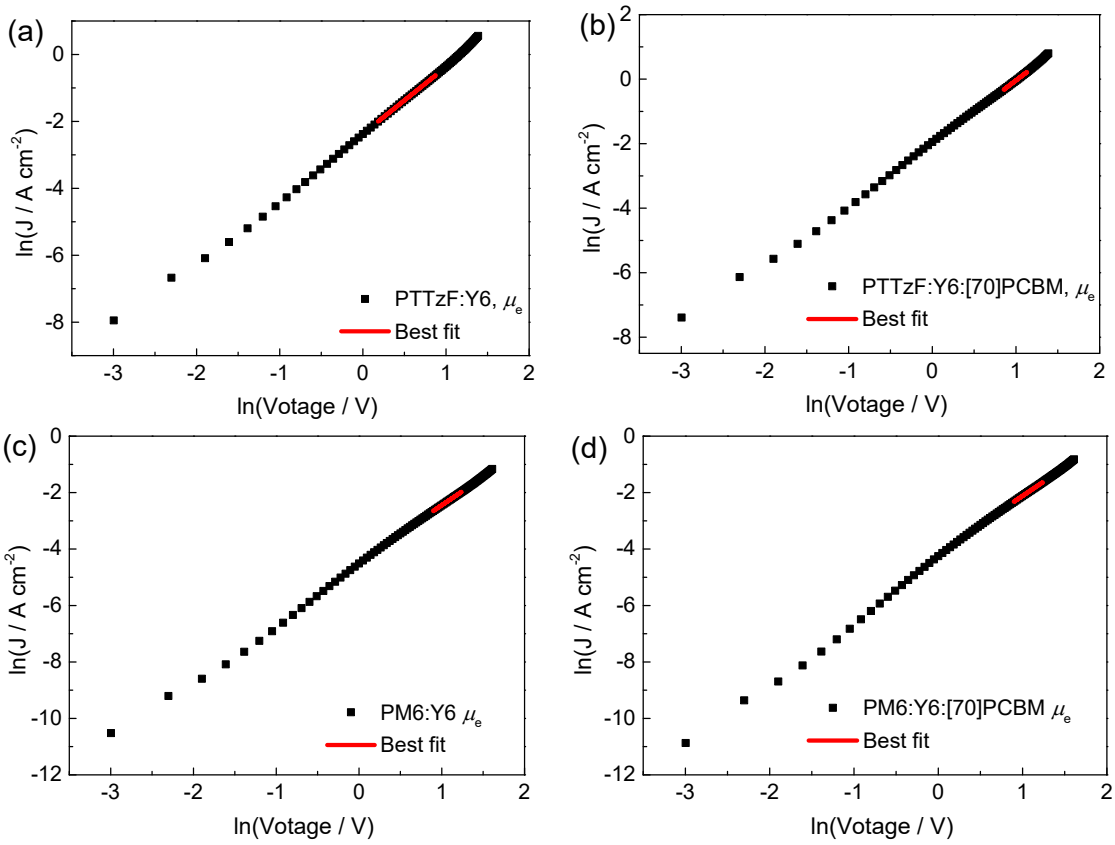

Figure S14. *J–V* characteristics of the electron-only devices based on the blend films of PTTzF and PM6.

Table S4. The mobility of the neat polymers and blend films at an electric field (E) of 1.0×10^5 V cm^{-1}.

Sample		μ_0 at zero electric filed [cm^2 V^{-1} s^{-1}]	γ [cm$^{1/2}$ V$^{-1/2}$]	μ at E = 1×10^5 V cm^{-1} [cm^2 V^{-1} s^{-1}]	μ_e/μ_h
PTTzF	μ_h	3.36×10^{-3}	-3.40×10^{-4}	3.02×10^{-3}	--
PM6	μ_h	1.35×10^{-3}	6.53×10^{-4}	1.66×10^{-3}	--
PTTzF:Y6	μ_e	1.55×10^{-3}	4.40×10^{-5}	1.57×10^{-3}	0.91
	μ_h	1.69×10^{-3}	7.71×10^{-5}	1.73×10^{-3}	
PTTzF:Y6:[70]PCBM	μ_e	2.25×10^{-3}	1.33×10^{-4}	2.35×10^{-3}	0.98
	μ_h	2.00×10^{-3}	5.54×10^{-4}	2.38×10^{-3}	
PM6:Y6	μ_e	1.10×10^{-3}	-1.54×10^{-4}	1.05×10^{-3}	0.85
	μ_h	1.01×10^{-3}	6.48×10^{-4}	1.24×10^{-3}	
PM6:Y6:[70]PCBM	μ_e	1.45×10^{-3}	6.90×10^{-5}	1.45×10^{-3}	0.88
	μ_h	1.37×10^{-3}	5.78×10^{-4}	1.64×10^{-3}	

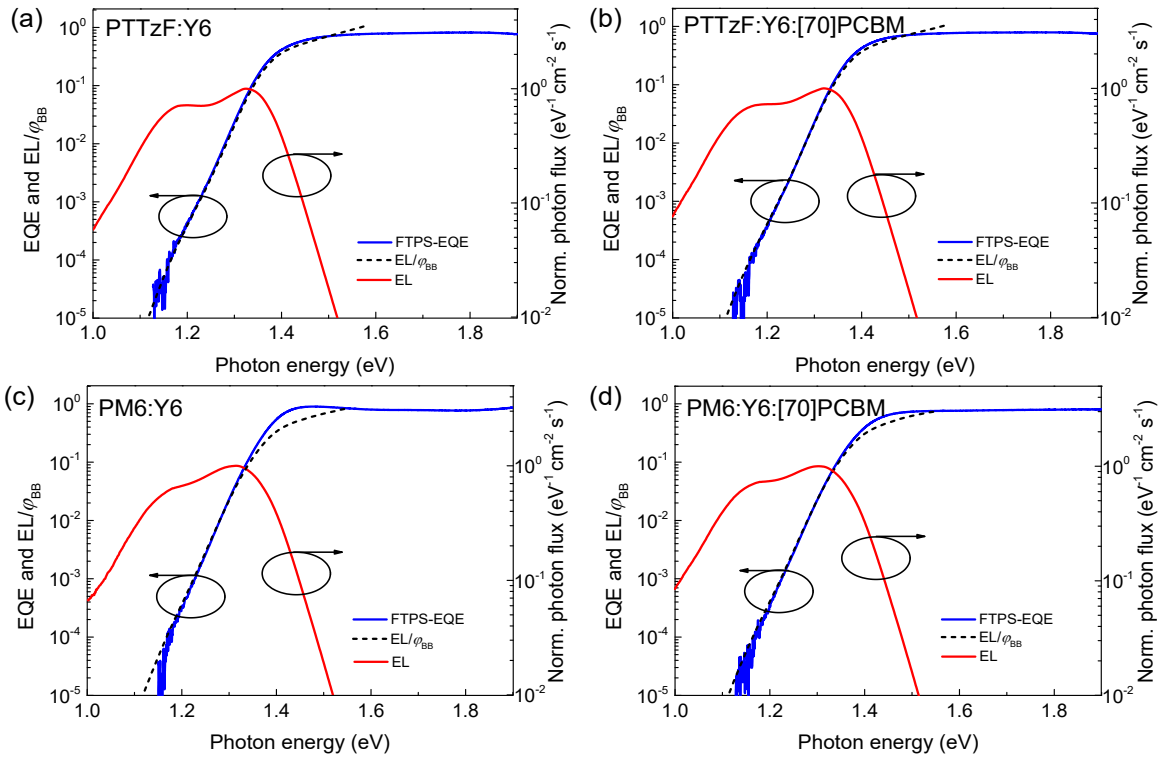

Figure S15. The highly sensitive EQE and EL spectra of the OSCs based on (a) PTTzF:Y6, (b) PTTzF:Y6:[70]PCBM, (c) PM6:Y6, and (d) PM6:Y6:[70]PCBM.

Table S5. The energy loss of the OSCs based on PTTzF and PM6.

Device	E_g (eV)	$qV_{OC,SQ}$ (eV)	$qV_{OC,Rad}$ (eV)	EQE_{EL} (%)	$\Delta E_{rad,SQ}$ (eV)	$\Delta E_{rad,tail}$ (eV)	ΔE_{nonrad} (eV)	ΔE_{loss} (eV)
PTTzF:Y6	1.40	1.14	1.08	1.70 × 10-2	0.26	0.06	0.22	0.54
PTTzF:Y6:[70]PCBM	1.40	1.14	1.08	1.80 × 10-2	0.26	0.06	0.22	0.54
PM6:Y6	1.39	1.13	1.08	7.10 × 10-3	0.26	0.05	0.25	0.56
PM6:Y6:[70]PCBM	1.40	1.14	1.08	1.10 × 10-2	0.26	0.06	0.24	0.56

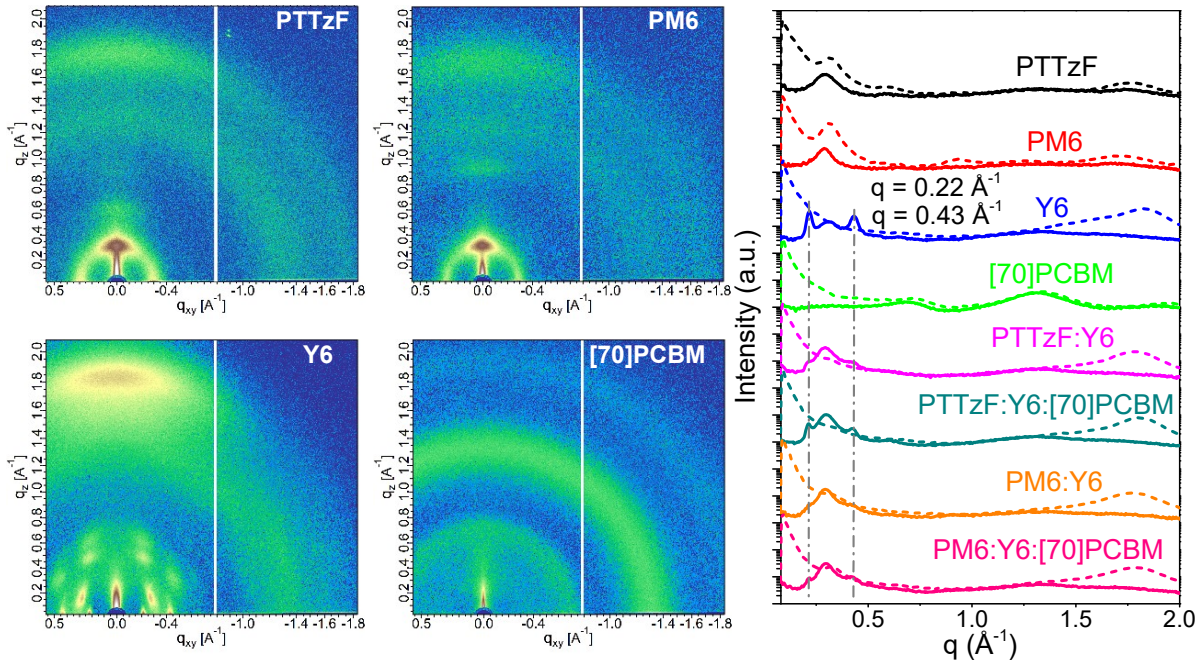

Figure S16. The 2D-GIWAXS patterns of the neat films of PTTzF, PM6, Y6, and [70]PCBM and 1D-GIWAXS line-cut profiles of the neat and blend films (Solid line: IP; dashed line: OOP).

Table S6. Lattice parameters of the neat films and blend films from GIWAXS measurement.

Sample	OOP (010) π–π stacking		IP (100) lamellar stacking	
	d-spacing [Å]	CCL [Å]	*d*-spacing [Å]	CCL [Å]
PTTzF	3.55	28	21.62	78
PM6	3.68	19	20.08	65
Y6	3.43, 3.63	36, 13	20.53, 14.54	56, 155
PTTzF:Y6	3.52	29	21.19	85
PTTzF:Y6:[70]PCBM	3.48	30	21.72	108
PM6:Y6	3.54	24	21.20	85
PM6:Y6:[70]PCBM	3.51	26	21.44	90

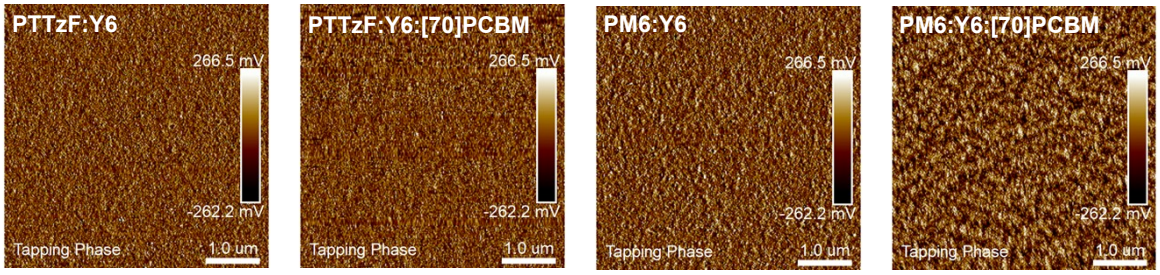

Figure S17. The AFM phase images of PTTzF:Y6, PTTzF:Y6:[70]PCBM, PM6:Y6, and PM6:Y6:[70]PCBM blends.

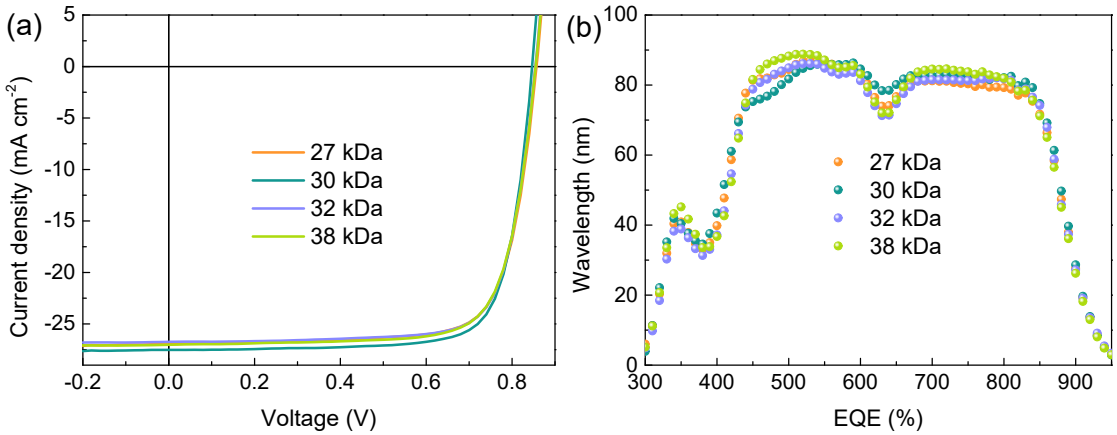

Figure S18. (a) The *J*–*V* curves and (b) EQE spectra of the PTTzF:Y6:[70]PCBM ternary OSCs with different batches of PTTzF.

Table S7. Device parameters of of the PTTzF:Y6:[70]PCBM ternary OSCs with different batches of PTTzF.[a)]

M_n (kDa)	V_{oc} (V)	J_{sc} (mA cm^{-2})	J_{sc} [b)](mA cm^{-2})	FF (%)	PCE (%)
27	0.857	26.99	25.78	0.755	17.47 (17.37±0.05)
30	0.847	27.52	26.28	0.773	18.01 (17.77±0.19)
32	0.854	26.73	25.72	0.766	17.49 (17.41±0.05)
38	0.855	27.02	26.08	0.757	17.48 (17.44±0.05)

[a)] Average values with standard deviation in brackets were acquired from at least eight independent devices.
[b)] The J_{sc} integrated from EQE spectra.

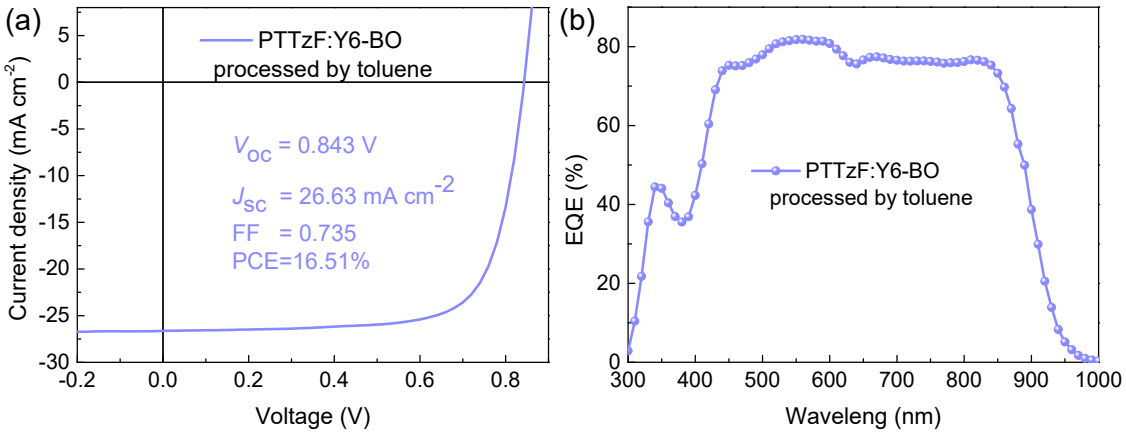

Figure S19. (a) The *J*–*V* curve and (b) EQE spectrum of the PTTzF:Y6-BO binary OSC processed from toluene.

References

1. S. Subramaniyan, H. Xin, F. S. Kim, S. Shoaee, J. R. Durrant and S. A. Jenekhe, *Adv. Energy Mater.*, 2011, **1**, 854-860.
2. P. Wan, C. An, T. Zhang, K. Ma, N. Liang, Y. Xu, S. Zhang, B. Xu, J. Zhang and J. Hou, *Polym. Chem.*, 2020, **11**, 1629-1636.
3. J. Hou, M.-H. Park, S. Zhang, Y. Yao, L.-M. Chen, J.-H. Li and Y. Yang, *Macromolecules*, 2008, **41**, 6012-6018.

4. D. Qian, L. Ye, M. Zhang, Y. Liang, L. Li, Y. Huang, X. Guo, S. Zhang, Z. a. Tan and J. Hou, *Macromolecules*, 2012, **45**, 9611-9617.
5. M. Zhang, X. Guo, W. Ma, H. Ade and J. Hou, *Adv. Mater.*, 2015, **27**, 4655-4660.
6. T. Rehman, Z.-X. Liu, T.-K. Lau, Z. Yu, M. Shi, X. Lu, C.-Z. Li and H. Chen, *ACS Appl. Mater. Interfaces*, 2019, **11**, 1394-1401.
7. J. Lee, D. H. Sin, J. A. Clement, C. Kulshreshtha, H. G. Kim, E. Song, J. Shin, H. Hwang and K. Cho, *Macromolecules*, 2016, **49**, 9358-9370.
8. Q. Liu, Y. Jiang, K. Jin, J. Qin, J. Xu, W. Li, J. Xiong, J. Liu, Z. Xiao, K. Sun, S. Yang, X. Zhang and L. Ding, *Sci. Bull.*, 2020, **65**, 272-275.
9. Y. Cui, Y. Xu, H. Yao, P. Bi, L. Hong, J. Zhang, Y. Zu, T. Zhang, J. Qin, J. Ren, Z. Chen, C. He, X. Hao, Z. Wei and J. Hou, *Adv. Mater.*, 2021, **33**, 2102420.
10. Y. Xu, Y. Cui, H. Yao, T. Zhang, J. Zhang, L. Ma, J. Wang, Z. Wei and J. Hou, *Adv. Mater.*, 2021, **33**, 2101090.
11. X. Liu, P. Cai, Z. Chen, L. Zhang, X. Zhang, J. Sun, H. Wang, J. Chen, J. Peng, H. Chen and Y. Cao, *Polymer*, 2014, **55**, 1707-1715.
12. C. Sun, F. Pan, H. Bin, J. Zhang, L. Xue, B. Qiu, Z. Wei, Z.-G. Zhang and Y. Li, *Nat. Commun.*, 2018, **9**, 743.